Taylor & Francis
Taylor & Francis Group

Variable zoom system with aberration correction capability

Yang Lu*, Christopher R. Stockbridge, Samuel M. Hoffman and Thomas G. Bifano

Mechanical Engineering, Boston University Photonics Center, 8 Saint Mary's Street, Boston, Massachusetts 02215, USA

We describe experiments conducted with two deformable mirrors (DMs) at fixed locations in an optical microscope imaging system. In this configuration, the DM shapes are controlled to provide 2.5× zoom capability, to allow dynamic focus control and to compensate for aberrations of the fixed optical components. Zoom is achieved by simultaneously adjusting focal lengths of the two DMs, which are inserted between an infinity-corrected microscope objective and a tube lens. Image quality is measured using contrast modulation, and performance of the system is quantified, demonstrating an improved point spread function in the adaptively compensated system.

1. Introduction

Compact deformable mirrors (DMs) make it possible to explore alternatives to conventional optical configurations for optical zoom, focus and aberration compensation. For example, high-speed optical zoom can be achieved using two DMs without axial translation of components. Active/adaptive zoom systems have been demonstrated previously by different groups using variable focal-length elements, such as flexible liquid-filled refractive elements [1–4], liquid crystal spatial light modulators (SLMs) [5,6] and low-order membrane deformable mirrors [7–13]. One potential advantage of an optical zoom system based on DMs or SLMs is the capacity to use higher-order shape control to compensate system aberrations in parallel with lower-order focus control to achieve image magnification or demagnification. With DMs, an added advantage is that the optical elements themselves are free of chromatic aberrations. This work focuses on a variable zoom system which will alter image magnification by reshaping the surface of the DMs to adjust image magnification up to 2.5×, while ensuring sharp focus and compensating aberrations in the optical path.

The primary approach chosen for shape control in this work is open-loop control of previously calibrated microelectromechanical system (MEMS) DMs, using Zernike polynomial shape functions as a basis set [14]. The use of Zernike polynomials has an advantage in this application since Zernike decomposition allows independent, decoupled control of defocus with respect to other optical aberrations. Moreover, the common off-axis aberrations observed in microscopy system (e.g. astigmatism, coma) are well represented by a compact set of lower-order Zernike polynomials.

2. MEMS DMs and open-loop controllability

A pair of continuous face-sheet MEMS DMs with 140 independent electrostatic actuators (Boston Micromachines Corporation MultiDM) was used in this study. Each DM features $3.5\,\mu m$ maximum stroke and $400\,\mu m$ pitch between actuator centers, which are arranged in a square 12 by 12 grid. At each of the four corners of the array is an inactive actuator. These DMs have been used widely in research related to adaptive optics in microscopy, astronomy and laser communication [15]. In the work reported here, these DMs were calibrated using a surface mapping interferometer (Zygo NewView 6300) prior to the experiments. Combined with a precise model of DM electromechanical behavior, this calibration allows accurate control of DM shape to within a few tens of nanometers root-mean-square error of a required shape without feedback [16,17]. Zernike shapes with up to $2.5\,\mu m$ amplitude were made with this approach and shape errors of $<25\,nm$ rms in most cases were reported [18]. The images presented in Figure 1 qualitatively show the capability of this calibrated controller.

The relationship between peak-to-valley magnitude, δ, of an imposed parabolic shape on the DM and
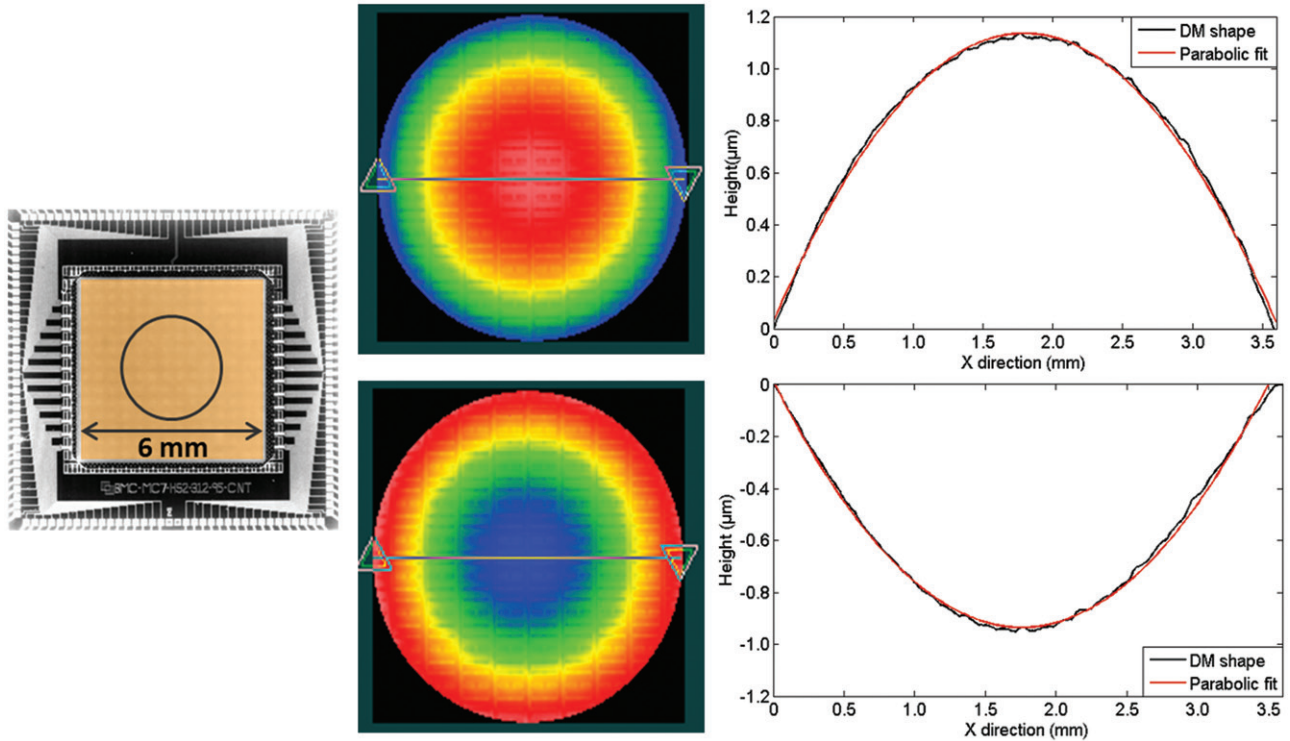
*Corresponding author. Email: luyang@bu.edu

Figure 1. DM defocus shapes made using the calibrated controller and measured using a surface mapping interferometer. Left: DM and its active aperture. Middle: −650 mm (top) and +900 mm (bottom) focal length defocus shapes. Right: cross-section view of the DM defocus shape with parabolic curve fit. (The color version of this figure is included in the online version of the journal).

the corresponding effective focal length f_{DM} is determined geometrically:

$$f_{DM} = \frac{D^2}{16\delta} \qquad (1)$$

where D is the diameter of the active mirror aperture. In this work, a circular optical aperture measuring 3.6 mm in diameter comprises the portion of the DM for which a specific shape control objective is defined. Actuators outside of that region are also controlled, to help achieve shape control objectives inside of the control aperture, by minimizing mirror forces at the aperture boundary. In the experiments presented here, the range of DM shapes used is limited to those having maximum mirror peak-to-valley displacement of 2.5 μm. With this constraint, the DM focal length can be varied from ±324 mm to ±∞. Both DMs are controlled through a MATLAB interface.

3. Experimental demonstration

3.1. Optical setup

An optical apparatus was constructed to demonstrate zoom, focus and aberration control (Figure 2).

A chrome-plated 1951 USAF resolution target was used as a reference object in all experiments. It features high-contrast line pairs spaced as closely as 645 line pairs/mm (1.5 μm separation between lines). A Nikon CF EPI 100×/0.95 infinity corrected objective was used as the primary microscope objective. The white light source was a white-light delivered through an optical fiber bundle (Coherent Inc.). A second high numerical aperture objective (Olympus LM Plan FL 100×/0.8 infinity corrected) was used subsequently (see Figure 5) to generate a diffraction-limited point source for the microscope in the aberration compensation experiments.

The back pupil plane of the objective was re-imaged to the first DM surface using two refractive lenses in a 4f configuration with unity magnification. Because this DM's surface is conjugate to the pupil plane of the objective, it can be used in a conventional adaptive optics control loop to compensate phase aberrations affecting the image plane. Consequently, all aberration compensation was performed using the first DM. The second DM was positioned 200 mm away from the first DM along the optical axis, followed by a 200 mm focal length lens and a CCD camera (UNIQ UP-1830CL).
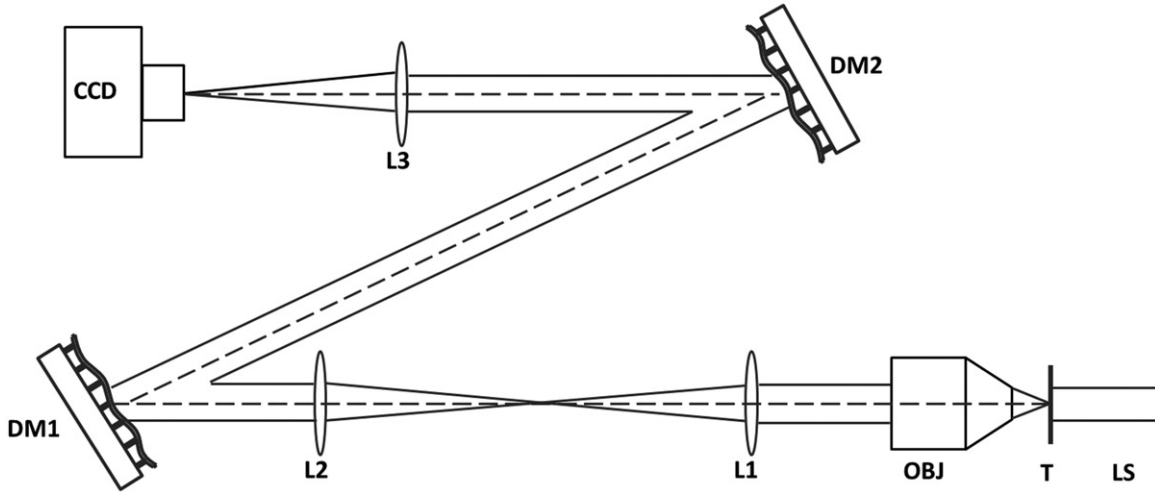
Figure 2. Variable zoom system schematic. LS: white light source, T: resolution target, OBJ: objective lens, L1–3: lenses, DM1–2: deformable mirrors, CCD: camera.

3.2. Zoom demonstration

The zoom module, comprised of two DMs, is designed to be an afocal beam magnifier. It simply expands or contracts an incident collimated beam. Parallel rays entering the system will exit as parallel rays, though the spacing between rays will vary with magnification, as shown in Figure 3.

Entering rays reflect from the first DM, travel in free space a distance s, and then reflect from the second DM. The ray optical propagation through the system can be modeled using matrix representation:

$$\begin{pmatrix} y' \\ \theta' \end{pmatrix} = \begin{pmatrix} 1 & 0 \\ -\frac{1}{f_2} & 1 \end{pmatrix} \begin{pmatrix} 1 & s \\ 0 & 1 \end{pmatrix} \begin{pmatrix} 1 & 0 \\ -\frac{1}{f_1} & 1 \end{pmatrix} \begin{pmatrix} y \\ 0 \end{pmatrix}, \quad (2)$$

$$y' = \left(1 - \frac{s}{f_1}\right) y + s\theta, \qquad (3)$$

$$\theta' = \left(\frac{s}{f_1 f_2} - \frac{1}{f_1} - \frac{1}{f_2}\right) y + \left(1 - \frac{s}{f_2}\right)\theta, \qquad (4)$$

where y and y' are input position and output position with respect to the optical axis, and θ and θ' are the input angle and output angle with respect to the optical axis.

For an afocal zoom, if $\theta = 0$ then $\theta' = 0$ for all y. Therefore, Equation (4) becomes:

$$\left(\frac{s}{f_1 f_2} - \frac{1}{f_1} - \frac{1}{f_2}\right) = 0. \qquad (5)$$

As a result, the operational constraint required for afocal zoom is:

$$f_1 + f_2 = s. \qquad (6)$$

Table 1. Magnification with different focal lengths when DM separated by 200 mm.

f_{DM1}(mm)	−324	−500	−1000	∞	1000	700	524
f_{DM2}(mm)	524	700	1200	∞	−800	−500	−324
M_z	−1.61	−1.40	−1.20	1.00	−0.80	−0.71	−0.62

The magnification M_Z and zoom ratio Z are:

$$M_z = -\frac{f_2}{f_1}, \qquad (7)$$

$$Z = \frac{M_{\max}}{M_{\min}}. \qquad (8)$$

Calculated magnifications are shown for several zoom settings in Table 1. Both DMs can have a minimum focal length of –324 mm. Note that the nominal magnification for the microscope configuration shown in Figure 2 is 100×. In Table 1, zoom magnification is referenced to this nominal system magnification. For example, $M_z = 2.5\times$ corresponds to system magnification of 250×.

A maximum zoom of ~2.5× is achievable. The resulting images of a 1951 USAF Resolution Target, Group 9 (line spacing minimum ~1.5 μm) are shown in Figure 4.

Note that the image becomes dimmer for larger zoom settings. This is expected, since the expanding beam reflected from the first DM is partly obscured by the aperture stop in front of the second DM for larger zoom magnifications.
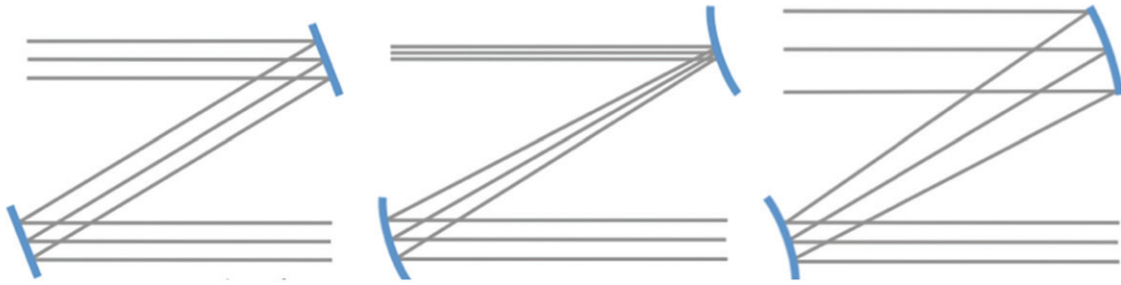
Figure 3. Zoom module schematic. Left: When both DMs are flattened, the magnification is 1. Middle: When the first DM is concave ($f > 0$), and the second DM collimates the beam, the magnification is < 1. Right: When the first DM is convex ($f < 0$), and the second DM collimates the beam, the magnification is > 1. (The color version of this figure is included in the online version of the journal).
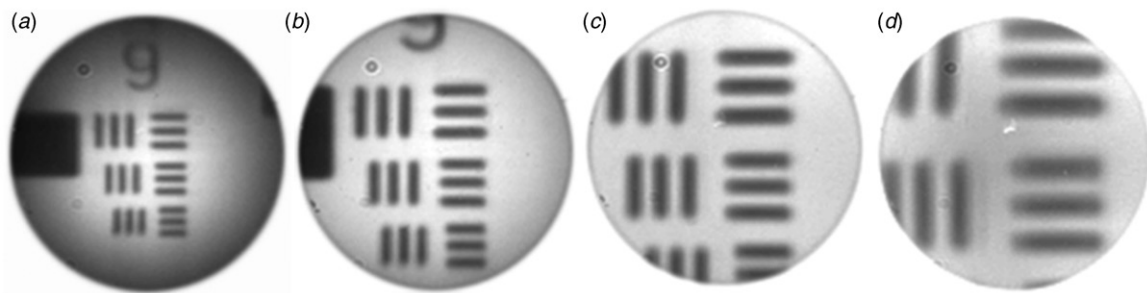

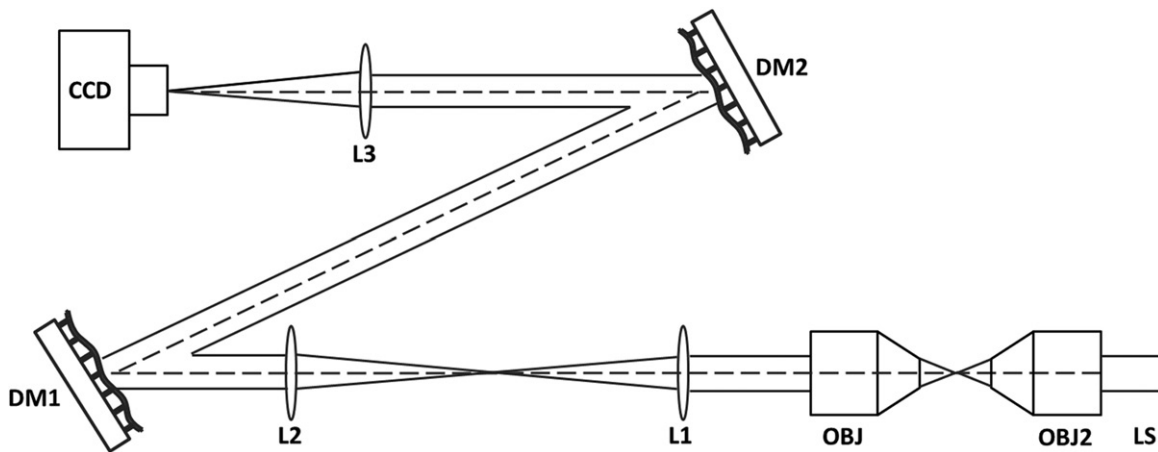Figure 4. (*a*) 1× Zoom; (*b*) 1.5× zoom; (*c*) 2× zoom; (*d*) 2.5× zoom.

Figure 5. Optical configuration for PSF aberration correction. LS: 633 nm collimated laser source, OBJ2: focusing objective lens, OBJ: objective lens, L1–3: lenses, DM1–2: deformable mirrors, CCD: camera.

3.3. *Point spread function (PSF) correction*

The optical setup was reconfigured (Figure 5) to demonstrate aberration compensation. Instead of imaging the USAF target, the target was removed and the illumination source replaced by a 633 nm wavelength collimated laser diode focused to a diffraction-limited Airy disk at the object plane of the microscope using a second objective lens. The illumination objective has a numerical aperture (NA) of 0.80, and would be expected to produce a diffraction limited Airy disk radius of 0.48 μm ($0.61\lambda M_z/$NA) at its image plane. At unity zoom magnification, the corresponding Airy disk image at the microscope camera should have a radius of 48 μm.

Strehl ratio – the ratio of measured peak intensity of an imaged point source to the ideal (diffraction-limited) peak intensity of the imaged point source in the absence of any aberrations – was used to evaluate performance of the system. Strehl ratio can vary from 0 to 1, and larger Strehl ratio corresponds to better optical quality. Often, a Strehl ratio of 0.8 or higher is considered to be indicative of a well-compensated optical system. We estimated the diffraction limited point spread function (PSF) peak intensity based on the ideal Airy function formula and the cumulative light intensity measured over a square area scanning approximately six times the Airy disk radius in both directions. Before compensation, the Strehl ratio of the point image was 0.52. The Strehl is less than one because the system incorporates several modest quality spherical singlet lenses and a folded optical path that introduces astigmatism. The first DM was subsequently used to increase Strehl ratio, using a blind optimization technique.

The metric chosen in this case was the peak intensity of the image, which correlates with Strehl ratio. Maximizing the value of this scalar metric was the objective for the optimization algorithm. The optimization method involved controlling the DM using linear combinations of low-order Zernike shapes while monitoring feedback based on this metric.

$$Q = I_{max}. \qquad (9)$$

Assuming that most of the aberrations in the system are of low order, we chose to shape the DM with only second-, third- and fourth-order Zernike shapes (astigmatism, focus, trefoil, coma and first-order spherical aberration) using calibrated open loop DM control. The optimization technique selected was a stochastic parallel gradient descent (SPGD) algorithm. SPGD is an optimization technique pioneered in adaptive optics in wavefront correction [19]. At iteration number n, the coefficient of each Zernike term C_n^i was perturbed by a small step $\Delta C_n^1 i$ in a random direction, $r_n^i = \pm 1$. Using these perturbed coefficients, the appropriate DM command inputs were calculated via previously stored calibration data. After applying the inputs to the DM, the image quality metric Q_n^+ was measured. Next, the perturbation sign was reversed and a second image quality metric Q_n^- was measured. Using integral feedback control based on the difference between measured metric values, an updated state for the Zernike coefficients was calculated as $C_{n+1}^i = C_n^i + G\Delta C_n^i r_n^i (Q_n^+ - Q_n^-)$, where G is the integral controller gain. This cycle was repeated iteratively until the measured metric converged to an optimal value. We found that with a gain of 0.5 and a perturbation step size of about 25 nm rms for each Zernike term, the
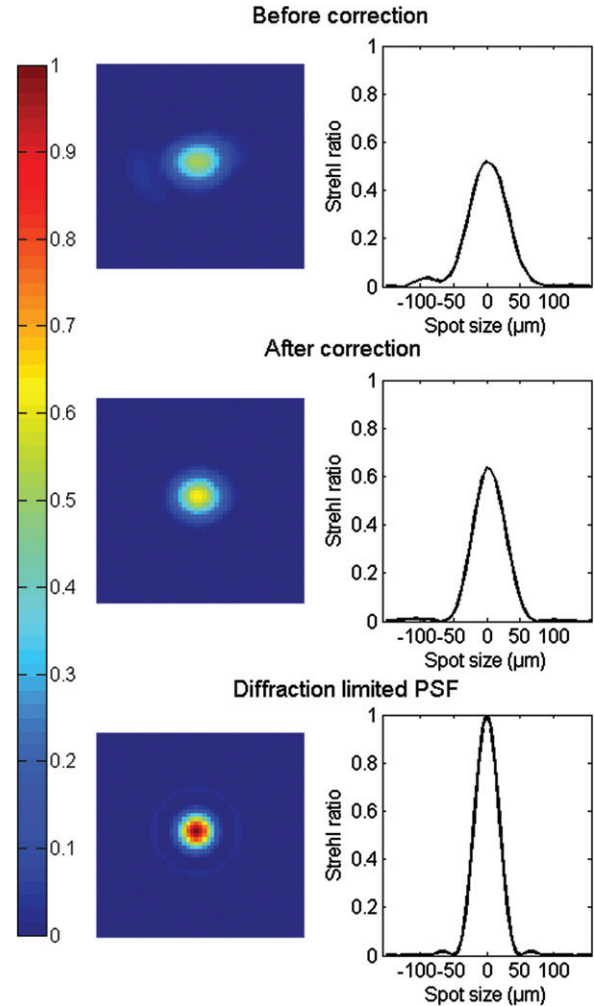

Figure 6. PSF comparison and line profile in X direction. (The color version of this figure is included in the online version of the journal).

SPGD algorithm converged within about 100 iterations. After optimization, we observed that the Strehl ratio increased to 0.64, as shown in Figure 6.

3.4. Aberration compensation on a USAF resolution target

We extended our optimization experiment to include real images as well, and inserted an artificial aberration source (+1.5 diopter trial lens) in the optical path to accentuate aberration.

In this case, we used contrast transfer function (CTF) in a small region of the image as our scalar quality metric.

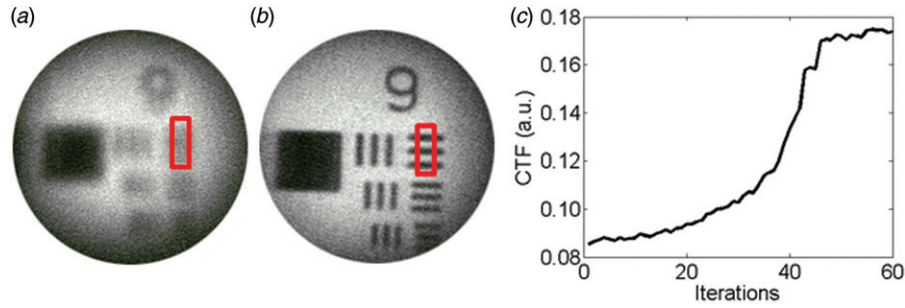$$\text{CTF} = \frac{I_{max} - I_{min}}{I_{max} + I_{min}}. \qquad (10)$$

Figure 7. Aberration compensation using SPGD voltage Zernike approach over the region of interest: (*a*) before correction; (*b*) after correction; (*c*) CTF vs. iteration. (The color version of this figure is included in the online version of the journal).

Table 2. Zernike decomposition of optimized DM shape.

Zernike term	Aberration name	Shape PV (nm)
3	Astigmatism X	−50
4	Defocus	1300
5	Astigmatism Y	−100
6	Trefoil X	−100
7	Coma X	0
8	Coma Y	0
9	Trefoil Y	50
12	Spherical	−50

With the same SPGD optimization approach and similar optimization parameters, we were able to optimize successfully, as shown in Figure 7. The CTF value was increased by a factor of two within 60 iterations.

We also implemented a stochastic serial gradient descent (SSGD) algorithm in which Zernike coefficients were optimized sequentially. Although slower than the SPGD optimization, this approach also led to convergence and optimization of about the same quality, and allowed easy calculation of component Zernike terms in the final DM shape. Table 2 shows a term-by-term Zernike decomposition of the final shape applied to the DM in the SSGD optimization.

We can use Equation (1) and the major defocus term PV to calculate the effective focal length of the DM. The 1300 nm peak-to-valley defocus shape on the optimized DM corresponds to a focal length of +623 mm, or +1.60 diopters, which is close to that of the artificially introduced aberration source.

complementary control of two DMs to achieve zoom, and then relies on one of the DMs to additionally compensate aberrations using an iterative optimization control loop. It is perhaps important to observe that focus is among the fundamental aberration terms that can be compensated in this system, allowing the optimization algorithm to ensure sharp imaging irrespective of zoom magnification. Aberrations, misalignments and off-axis beam path errors can be compensated using the DM that is conjugate to the objective's back pupil plane.

A limitation of the system described is its relatively small range of zoom magnification (2.5×). Fundamentally, this is related to DM focal length range: shorter achievable focal lengths in the DMs lead to larger achievable system zoom magnifications. Two ways to achieve shorter focal lengths are to increase the achievable stroke of the DM or to reduce its diameter. A survey of commercially available DMs with continuous membrane surfaces yields off-the-shelf products that can produce focal lengths as small as 60 mm, which should be sufficient to produce zoom magnifications of up to 9× in the geometric configuration used here. Also, a system with larger DM separation will produce larger zoom ratio, at a cost of system compactness.

An inherent advantage of using compact MEMS DMs in this application is the prospect of achieving zoom adjustment at unprecedented speeds. Since the update rate of the DM shape for the devices used in this work exceeds 3 kHz, open loop settling to a new zoom condition can be achieved within fractions of a millisecond.

4. Discussion and conclusions

In the experimental demonstrations described in this paper, a power-variable zoom system with dynamic aberration compensation capability has been demonstrated. The configuration allows coordinated

References

[1] Feng, G.H.; Chou, Y.C. *Appl. Opt.* **2009,** *48,* 3284–3290.

[2] Ren, H.; Wu, S.T. *Opt. Express* **2007,** *15,* 5931–5936.

[3] Zhang, D.Y.; Justis, N.; Lo, Y.H. *Opt. Lett.* **2004,** *29,* 2855–2857.

[4] Peng, R.; Chen, J.; Zhuang, S. *J. Opt. Soc. Am. A* **2008,** *25,* 2644–2650.

[5] Iemmi, C.; Campos, J. *J. Eur. Opt. Soc. Rap. Public.* **2009,** *4,* 09029.

[6] Tam, E.C. *Opt. Lett.* **1992,** *17,* 369–371.

[7] Wick, D.V.; Martinez, T. *Opt. Eng.* **2004,** *43,* 8–9.

[8] Dickensheets, D.L. *J. Micro/Nanolithogr., MEMS, MOEMS* **2008,** *7,* 021008–021009.

[9] Himmer, P.A.; Dickensheets, D.L.; Friholm, R.A. *Opt. Lett.* **2001,** *26,* 1280–1282.

[10] Vdovin, G. *Opt. Commun.* **1997,** *140,* 187–190.

[11] Wang, J.L.; Chen, T.Y.; Liu, C.; Chiu, C.W.E.; Su, G.D.J. *Elec. Telecom Res. Inst.* **2007,** *29,* 817–819.

[12] Martinez, T.; Wick, D.V.; Payne, D.M.; Baker, J.T.; Restaino, S.R. *Proc. SPIE* **2004,** *5234,* 375–378.

[13] Krogmann, F. *J. Opt. A: Pure Appl. Opt.* **2006,** *8,* S330–S336.

[14] Noll, R.J. *J. Opt. Soc. Am.* **1976,** *66,* 207–211.

[15] Bifano, T. *Nat Photonics* **2011,** *5,* 21–23.

[16] Vogel, C.; Tyler, G.; Lu, Y.; Bifano, T.; Conan, R.; Blain, C. *J. Opt. Soc. Am. A* **2010,** *27,* 56–63.

[17] Stewart, J.B.; Diouf, A.; Zhou, Y.P.; Bifano, T.G. *J. Opt. Soc. Am. A.* **2007,** *24,* 3827–3833.

[18] Diouf, A.; LeGendre, A.P.; Stewart, J.B.; Bifano, T.G.; Lu, Y. *Appl. Opt.* **2010,** *31,* G148–G154.

[19] Vorontsov, M.A.; Sivokon, V.P. *J. Opt. Soc. Am.* **1998,** *15,* 2745–2758.